

# Digital Mirror Devices in Optical MIMO Transmission

Peter Bartmann<sup>1</sup>, Andreas Ahrens<sup>2</sup>, Steffen Lochmann<sup>3</sup>, Ingo Müller<sup>4</sup>

Hochschule Wismar, University of Technology, Business and Design,  
Philipp-Müller-Straße 14, 23966 Wismar, Germany

<sup>1</sup>peter.bartmann@hs-wismar.de, <sup>2</sup>andreas.ahrens@hs-wismar.de

<sup>3</sup>steffen.lochmann@hs-wismar.de, <sup>4</sup>ingo.mueller@hs-wismar.de

## Abstract

From information theory the capacity of a Multi Mode Fiber (MMF) is higher than of a Single Mode Fiber (SMF). One opportunity to increase transmission rates in these fibers is to setup an optical Multiple Input Multiple Output (MIMO) system. In previous works we used eccentric splices to excite specific groups of modes. Now we replace the splices by a Digital Light Processor<sup>®</sup> (DLP). Physically, the micro mirror array in a DLP can be described as a blazed grating. The mathematical description is made using the Direction Cosine Space (DCS). We are able to calculate intensity distributions of reflected light in front of the Digital Micromirror Device (DMD) for any operation wavelength. With this knowledge we show how two independent light sources can be arranged in front of the DLP such that the reflected light waves have a common output direction, where an optic focuses and launches them into a MMF initiating different mode groups.

## 1 Introduction

Optical MIMO systems are investigated throughout the last decade, e.g., in several experimental papers [1–3]. The need of such systems cannot be discussed away due to the exponential grow of data traffic in optical metro and core networks [4–6]. Time division, wavelength and polarization multiplexing as well as high order modulation schemes has been developed coping with this demand and has reached a state of majority. Therefore, there exists a deep interest in Optical Space Division Multiplexing (OSDM). Still, how to launch physically multiple datastreams using the same lights wavelength into a fiber and separate them at the output is an open question next to the signal processing site. One approach is using Spatial Light Modulation (SLM) to excite several mode groups in serial, another one this paper is focusing on is using micro mirror arrays to excite low order and high order modes with two different sources in parallel.

The breakthrough of the DLP technology can be traced back to efforts made by Texas Instruments (TI) at beginning of the eighties, more precisely to Larry J. Hornbeck. The heart of a DLP projector is the DMD, which is patented by TI in 1986.<sup>1</sup> The DMD consists of thousand of small mirrors having sizes in micrometer domain. The principle of a DMD is quite simple: each mirror can be tilted such that incoming light is reflected either to an optical output system or to an absorber. Each mirror is a pixel in an image and can be switched on and of by reflecting incoming light to the output or the absorber. As this system is a combination of mechanical and electronic elements, it is also called a Micro Electro Mechanical System (MEMS).

In previous works we developed a Field Programmable Gate Array (FPGA) based system to handle the DLP1700 completely without the need of TI's own steering and driver chips [7, 8]. Hence, we can use the DLP1700 such that selected mode groups on a MMF's surface are excited. This paper describes how with this technique we are able to impinge two independent laser beams on the DMD's surface such that each laser beam excites different mode groups into one MMF in parallel. Hence, a  $M \times 2$  MIMO system is emphasized. This is a main advantage compared to other SLM techniques, e.g., as used in [9], as there are only able to expose a MIMO system in a serial way similar we did with excentric splices in [10].

This article deals with the description of our optical system from the two light sources to the MMF's surface. We will show, how the components have to be placed by using known mathematics and consequentially show up, where difficulties lie. Sec. 2 starts with a coarse description of the system itself. Sec. 3 describes the heart of our system – the DLP1700. From Sec. 2 and Sec. 3 we have all tools to develop an optimization program. Sec. 4 consequentially determines the optimal positioning of the our system components such that the overall power loss of the light sources is minimized. Finally Sec. 5 closes with a short conclusion and give an overview on upcoming work.

## 2 Experimental Setup

### 2.1 Modifying the Principle Structure of a DLP<sup>®</sup>-controlled System

Our basic strategy to exploit a mode selective launch into a MMF comes from the principle structure of a DLP technology driven modern digital video projector. The following picture captures how a DMD is embedded into such a video projector.

Fig. 1(a) shows the overall structure and Fig. 1(b) a simplified structure with just two pixel elements, respectively. Starting with the lamp producing white light, this light is firstly filtered by a color wheel and then focused with relay optics. Now the light waves interfaces the DMD's surface. In Fig. 1(b) one can clearly see that each mirror, i.e., each pixel, can be individually tilted to  $-\varrho$  and  $+\varrho$  such that the incoming light is reflected

---

<sup>1</sup>U.S. Patent 4,615,595

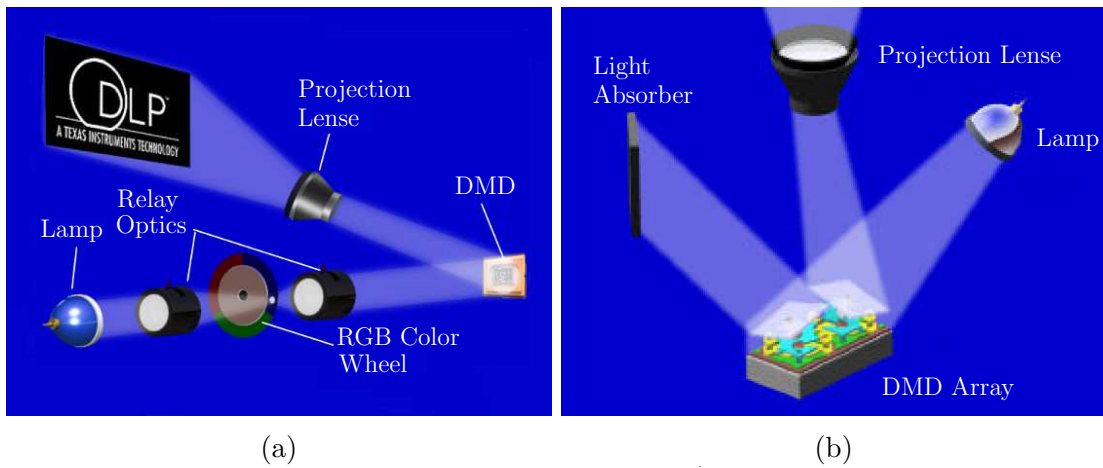


Figure 1: Principle structure of a digital video projector [11]

to the projection lens or to an absorber. This strategy is modified as follows: we wish to use the 'binary' tilt such that we are able to reflect two individual light beams placed on opposite sites in front of the DLP. This principle is sketched in Fig. 2.

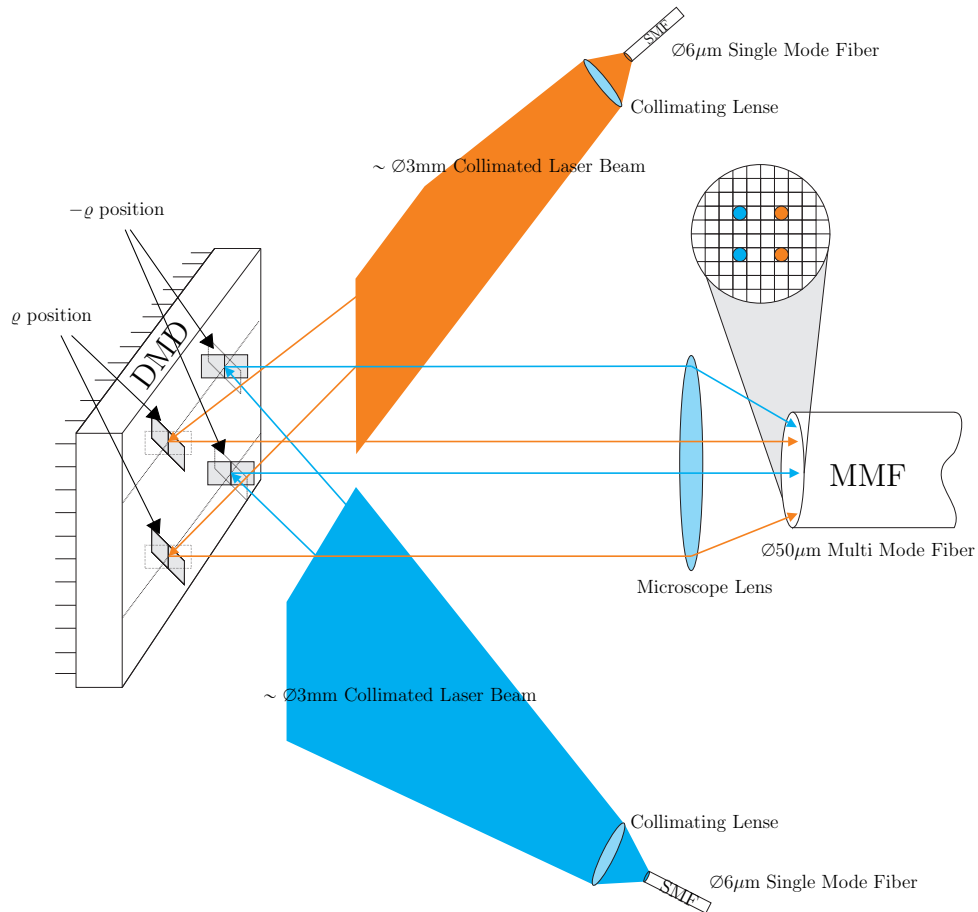


Figure 2: Strategy of assembling an optical MIMO system [7]

Here one can see that on each site light carrying the information to transmit was propagated through a SMF. At the end of the fiber the light is widened through a collimator directing towards on the DMDs surface. The DLP reflects the light from both sources to a common output direction where an optic which focuses the summation on a MMF's surface. By tilting each pixel individually to either  $-\rho$  or  $+\rho$  one is able to decide at this

point which source excite which mode groups at the MMF. Hence, by initializing the DLP with a certain bit map onto the micro mirrors, specific mode groups are stimulated at the MMFs surface, i.e., two different mode groups carrying two independent information streams down the MMF. This constructs the input coupling side of a  $M \times 2$  optical MIMO system.

The main problem is that the reflected light wave direction has to be equal for both input light waves. This means, the direction, where the lights intensity goes to, has to be equal for both sources with the only difference that the tilt is inverted. To determine the optimal positioning system, the nature of the DLP has to be considered as a blazed grating. Before we start with that mathematical description in Sec. 3 the following subsection defines an appropriate coordinate system first.

## 2.2 Defining a Coordinate System

We suggest to apply the calculation in the DCS as this coordinate system considers the output direction best. The center of the DMD lies in the origin of that system and the normal of the surface shows into  $\gamma'$  direction. We will call the other axes of this DCS  $\alpha'$  and  $\beta'$ , who are oriented with the micro mirror array. Fig. 3 clarifies its orientation.

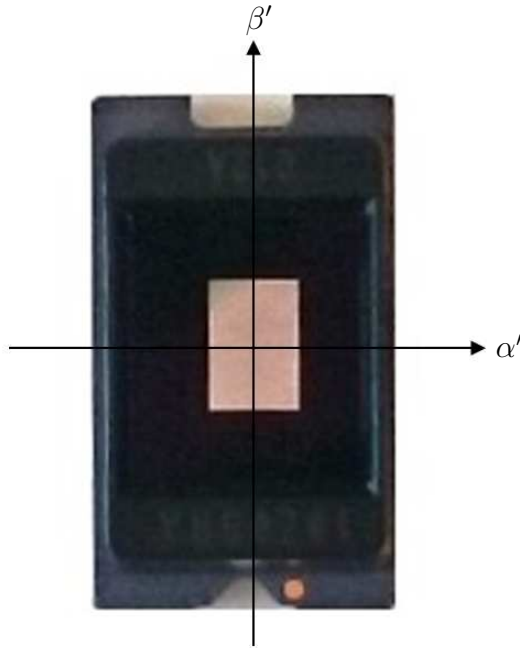


Figure 3: Coordinates of the direction cosine space of the DLP1700

Although the calculation in that system is quite easy done, one cannot use it directly. The optical positioning system is build up onto an optical breadboard. For simplification the collimators will be placed symmetrically arranged in front of the DLP1700, which will be the origin of the second coordinate system as well. In this DCS we call the axes  $\alpha$ ,  $\beta$  and  $\gamma$ . The system is orientated as depicted in Fig. 4.<sup>2</sup>

Fig. 4 partly shows our experimental setup using a second DCS indicated by its components  $\alpha$ ,  $\beta$  and  $\gamma$  and further defines three additional angles  $\varepsilon$ ,  $\theta$  and  $\varphi$ . The angel  $\varepsilon$

---

<sup>2</sup>Only one collimator is placed in that picture, whereas the second is missing.

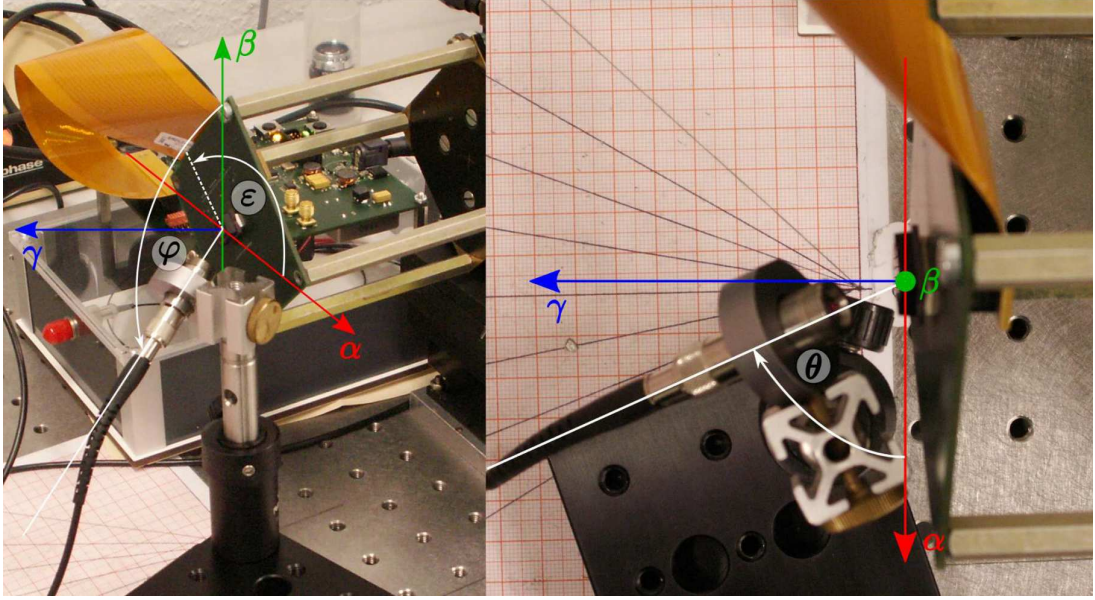


Figure 4: Experimental setup and its coordinates of the direction cosine space with one light source

describes the rotation of the DLP within the  $\alpha\beta$ -plane. This rotation is needed as the normal of each micro mirror has to be tilted parallel to the  $\alpha\gamma$ -plane. Therefore,  $\varepsilon$  equals either  $3/4 \pi$  or  $-1/4 \pi$  [12]. This angle also defines the connection between the two DCSs explained above. We use the well known rotation matrix

$$R = \begin{bmatrix} \cos \varepsilon & -\sin \varepsilon \\ \sin \varepsilon & \cos \varepsilon \end{bmatrix}$$

to get

$$\begin{pmatrix} \alpha \\ \beta \end{pmatrix} = R \begin{pmatrix} \alpha' \\ \beta' \end{pmatrix} \quad (1a)$$

and

$$\gamma = \gamma' . \quad (1b)$$

The other two angles  $\theta$  and  $\varphi$  are used to describe the inputting laser beam.  $\theta$  measures the angle between the  $\alpha\beta$ -plane and the input direction and  $\varphi$  to the  $\beta$ -axis.<sup>3</sup> Within the positioning system one is able to measure locations  $(x, y, z)^T$ . Assuming the vector  $(x_0, y_0, z_0)^T$  refers to one collimator center one may determine the angles by

$$\cos(\theta_i) = \frac{x_0}{\sqrt{x_0^2 + z_0^2}} \quad (2a)$$

$$\cos(\varphi_i) = \frac{y_0}{\sqrt{x_0^2 + y_0^2 + z_0^2}} \quad (2b)$$

One can see that (2b) is the  $\beta$ -component of the corresponding DCS by definition. Further,

<sup>3</sup>Parameters of incoming light direction are later marked with subscripts  $i$ ,  $i1$  and  $i2$ .

by using  $1 = \sin^2 \psi + \cos^2 \psi$  and combining (2a) and (2b) one can directly show that

$$\begin{aligned}\alpha_i &= \cos(\theta_i) \sin(\varphi_i) \\ \beta_i &= \cos(\varphi_i)\end{aligned}\tag{3}$$

follows. To complete this section, if there is a second collimator located in front of the DMD, symmetry means that

$$\begin{aligned}\theta_{i2} &= \pi - \theta_{i1} \\ \varphi_{i2} &= \varphi_{i1}\end{aligned}\tag{4}$$

holds where  $(\theta_{i1}, \varphi_{i1})$  relates to one collimator and  $(\theta_{i2}, \varphi_{i2})$  to the other one.

### 3 The Digital Light Processor<sup>®</sup> DLP1700

This section shows how the intensity distribution of the reflected light caused by diffraction is calculated for any operation wavelength  $\lambda$  as a function of the incoming direction of the laser beam to the DMD. The basic principles of the description are derived in [8, 13, 14]. The following calculation presumes that the intensity distribution is observed within the far field.

#### 3.1 Common Diffraction Grating

First we want to look at the DLP1700 as a common diffraction grating. The distribution can be easily described on a half sphere over the DMD in the DCS. If one look on the DLP1700 as a diffraction grating, one recognizes that a two dimensional adaptation of the light intensity distribution given in [13] leads to

$$I_D(\alpha', \beta', \alpha'_i, \beta'_i) = I_0 \left( \frac{\sin \left( P_{\alpha'} \pi \frac{d_{\alpha'}}{\lambda} (\alpha' + \alpha'_i) \right)}{P_{\alpha'} \sin \left( \pi \frac{d_{\alpha'}}{\lambda} (\alpha' + \alpha'_i) \right)} \right)^2 \left( \frac{\sin \left( P_{\beta'} \pi \frac{d_{\beta'}}{\lambda} (\beta' + \beta'_i) \right)}{P_{\beta'} \sin \left( \pi \frac{d_{\beta'}}{\lambda} (\beta' + \beta'_i) \right)} \right)^2, \tag{5}$$

where  $I_0$  is an intensity normalization factor and  $P_{\alpha'}$  and  $P_{\beta'}$  are the pixels of the DMD seen by the incoming light in  $\alpha'_i$ - and  $\beta'_i$ -direction, respectively. The constants  $d_{\alpha'}$  and  $d_{\beta'}$  are the grating constants with  $d_{\alpha'} = d_{\beta'} = 7.6 \mu\text{m}$  as given in [12]. Further, if we look on the maximums of that function, (5) becomes  $I_0$  for

$$\begin{aligned}\alpha'_m &= \left( m \frac{\lambda}{s_{\alpha'}} \right) - \alpha'_i \\ \beta'_n &= \left( n \frac{\lambda}{s_{\beta'}} \right) - \beta'_i\end{aligned}\tag{6}$$

Recalling the solution in [8]

$$\begin{aligned}\alpha_{m,n} &= \left(n \frac{\lambda}{s_{\alpha'}}\right) \sin\left(\varepsilon - \frac{\pi}{2}\right) + \left(m \frac{\lambda}{s_{\alpha'}}\right) \sin(\varepsilon) - \alpha_i \\ \beta_{m,n} &= \left(n \frac{\lambda}{s_{\beta'}}\right) \cos\left(\varepsilon - \frac{\pi}{2}\right) - \left(m \frac{\lambda}{s_{\beta'}}\right) \cos(\varepsilon) - \beta_i\end{aligned}\quad (7)$$

this is the same result simply connected by (1a). Due to the rotation the orders  $m$  and  $n$  are mixed up.

However, later it is important to use the full intensity distribution rather than simply the maximums. In the next step we look on the impact by the blazed grating characteristic introduced by the tilt of the micro mirrors.

### 3.2 Blazed Grating

The closed form solution of the blazed grating of a DLP is given in [14, p. 6].<sup>4</sup>

$$\text{sinc}^2\left[\frac{s_{\alpha'}}{\lambda}(\alpha' - \alpha'_i)\right] \text{sinc}^2\left[\frac{s_{\beta'}}{\lambda}(\beta' - \beta'_i)\right]$$

The constants  $s_{\alpha'}$  and  $s_{\beta'}$  are width and length of a pixel. They are indirectly given in the datasheet of the DLP1700 by the pitch and array fill factor to  $s_{\alpha'} = s_{\beta'} = 7.29\mu m$  [12]. However, to use that directly some precalculations has to be applied in advance. Fig. 5 defines some angles we use for that.

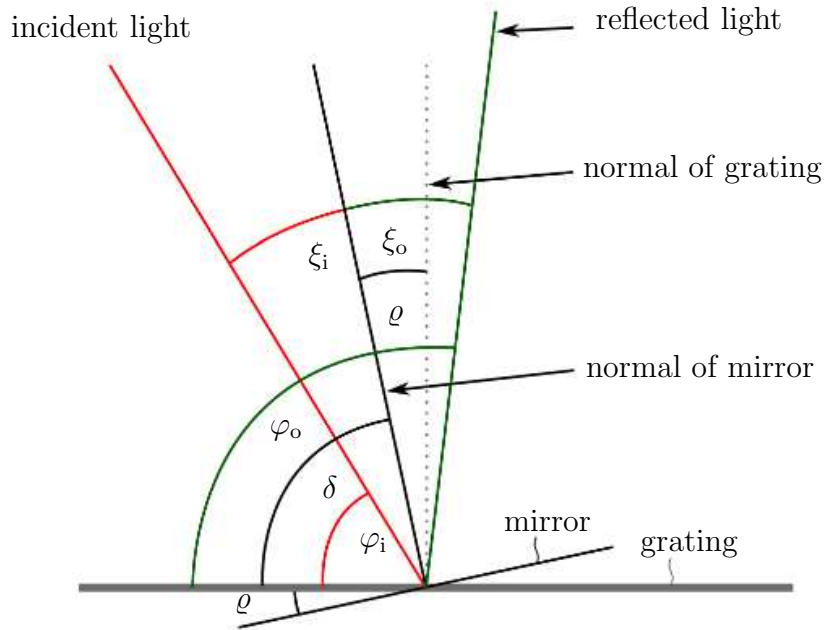


Figure 5: DMD as blazed grating – important angles

The output angle  $\varphi'$  is defined by the tilt of the micro mirrors  $\varrho$  and input angle  $\varphi$ .

$$\varphi' = \pi - \varrho - \varphi \quad (8)$$

<sup>4</sup>In contrast to the reference we use the  $\text{sinc}(\cdot)$  as classically defined.

An additional angle not shown in Fig. 5 is the angle between the projection of the mirrors normal on the gratings plane and the DMDs vertical axis called  $\eta$ . Hence,  $\eta$  equals  $\mp 3/4 \pi$  if the mirror is tilted to  $\varrho = \pm \pi/15$ . Now it is possible to determine the components of the mirrors normal in the DCS.

$$\begin{aligned}\alpha_{\text{MD}} &= \sin(\varrho) \cos(\eta) \\ \beta_{\text{MD}} &= \sin(\varrho) \sin(\eta)\end{aligned}\tag{9}$$

Finally, the DCS components of the reflected light are

$$\begin{aligned}\alpha_o &= \cos(2 \cdot \arccos(\alpha_{\text{MD}}) - \theta_i) \\ \beta_o &= \cos(2 \cdot \arccos(\beta_{\text{MD}}) - \varphi_i)\end{aligned}\tag{10}$$

The direction (10) gives the direction of the maximum of the intensity distribution function.

One have to keep in mind the rotation of the DLP by  $\varepsilon$  in the experimental setup. For an easier applicable formula, one may apply the same trick as above and rotate  $(\alpha_o, \beta_o)$  into the DMDs own DCS.

$$\begin{pmatrix} \alpha'_{\text{blazed}} \\ \beta'_{\text{blazed}} \end{pmatrix} = R^{-1} \begin{pmatrix} \alpha - \alpha_o \\ \beta - \beta_o \end{pmatrix}\tag{11}$$

Finally, the intensity distribution function of the blazed grating is defined as

$$I(\alpha', \beta', \alpha'_i, \beta'_i) = I_D(\alpha', \beta', \alpha'_i, \beta'_i) \text{sinc}^2\left(\frac{s\alpha'}{\lambda} \alpha'_{\text{blazed}}\right) \text{sinc}^2\left(\frac{s\beta'}{\lambda} \beta'_{\text{blazed}}\right),\tag{12}$$

where  $I_D(\alpha', \beta', \alpha'_i, \beta'_i)$  is the intensity distribution due to the common diffraction grating (5). In Fig. 6 the distribution for a one dimensional blazed grating over  $\alpha'$  is shown.  $I_B$  denotes the term above without considering the factor  $I_D$ .

### 3.3 Housing

As to be seen in datasheet of the DLP1700 the micro mirror array is build in an housing, which cannot be removed [12]. The array is placed directly on the housings ground and above of the array there is a window having black borders. The window is approximately 1.1mm above the micro mirrors surface. Due to the window above the aperture the Line of Sight (LOS) from the collimator lens to the micro mirror array might restricts the array size seen. The angles of a non-restricted view is a function of three parameters: the arrays dimension  $l_{\text{dmd}} \times w_{\text{dmd}}$ , the windows height  $w_{\text{dmd}}$  and the windows dimension. The first two parameters are described in the datasheet of the DLP1700 as well. They are given

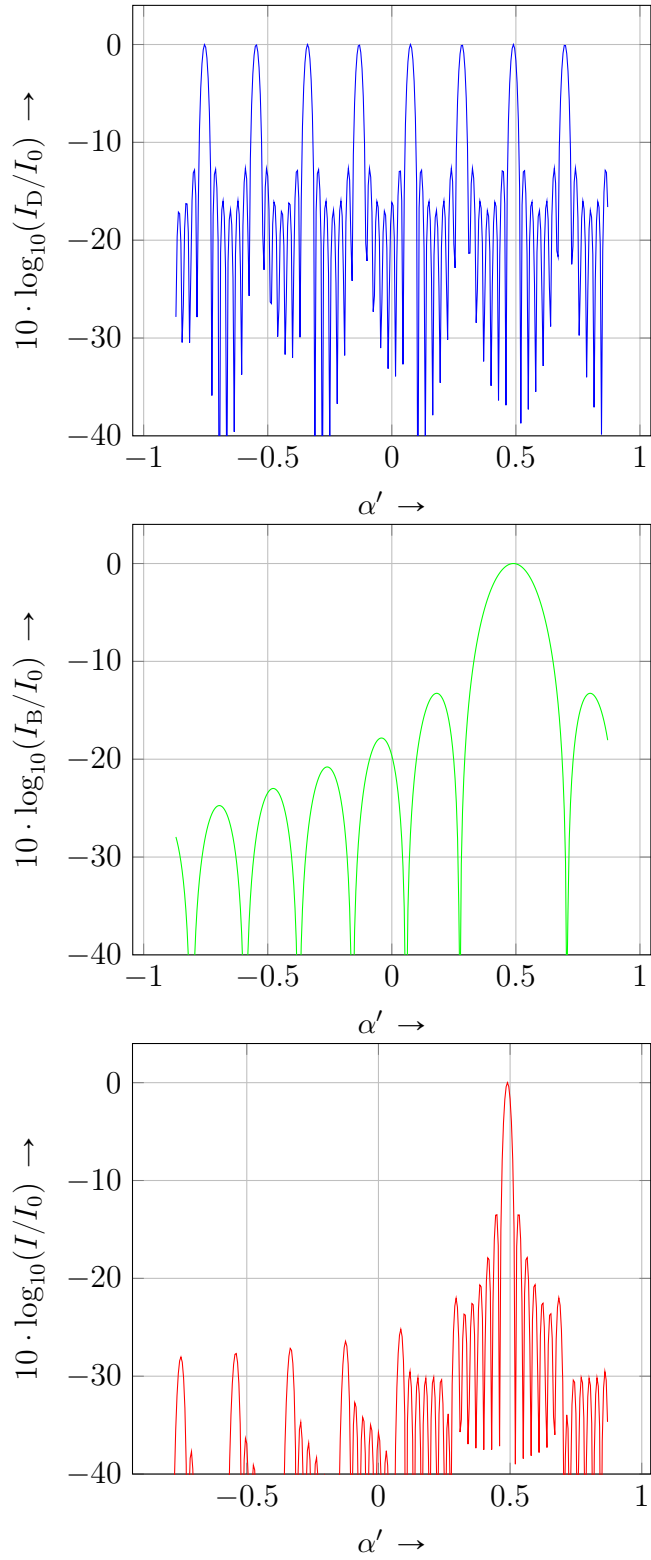


Figure 6: Intensity distribution for one dimension over  $\alpha'$  with  $P_{\alpha'} = 7$

by

$$\begin{aligned} l_{\text{dmd}} &= 480 \times 7.6\mu\text{m} - (7.6\mu\text{m} - 7.29\mu\text{m}) \\ &\approx 3.6478\text{mm} \end{aligned} \tag{13a}$$

$$\begin{aligned} w_{\text{dmd}} &= 320 \times 7.6\mu\text{m} - (7.6\mu\text{m} - 7.29\mu\text{m}) \\ &\approx 2.4318\text{mm} \end{aligned}$$

$$h_{\text{window}} = 1.11\text{mm}(\pm 0.084\text{mm}) \tag{13b}$$

For the calculation of the window size as well as the DMDs position beneath we took pictures directly from above the DLP. In these pictures we were able to calculate the missing parameters we are interested in. In detail, it is important to know the distances between the array ends and the corresponding window-edge.<sup>5</sup>

$$\begin{aligned} d_{\alpha'+} &\approx 0.69\text{mm} \\ d_{\alpha'-} &\approx 0.48\text{mm} \\ d_{\beta'+} &\approx 0.48\text{mm} \\ d_{\beta'-} &\approx 0.71\text{mm} \end{aligned} \tag{13c}$$

Having these values the calculation of the maximum non-restricted view angle on the DLP1700 is fairly easy if one presumes that the collimator distance from the DLP is much larger than  $h_{\text{window}}$ . By defining the directions

$$\begin{aligned} \vec{r}_{\alpha'} &= (d_{\alpha'\pm}, 0, h_{\text{window}})^T \\ \vec{r}_{\beta'} &= (0, d_{\beta'\pm}, h_{\text{window}})^T \end{aligned} \tag{14}$$

in the corresponding Cartesian space and by using the definition of the DCS one can specify the values

$$\begin{aligned} \alpha'^+ &\approx 0.53 \\ \alpha'^- &\approx -0.40 \\ \beta'^+ &\approx 0.40 \\ \beta'^- &\approx -0.54 \end{aligned} \tag{15}$$

as the maximum angles allowed where the LOS can see the whole micro mirror array. One have to keep in mind that these values hold if the direction is exactly from the  $\alpha\gamma$ - or on the  $\beta\gamma$ -plane, respectively. If one look from somewhere, i.e., not exactly from one of the two planes, the 'full-vision' area is approximated by quarters of ellipses. This result is given in Fig. 7 as well as how the area increases if one allow a certain restriction, i.e., that at least only a minor area of the DMD has to be seen from each input direction.

---

<sup>5</sup>Exchanging the DLP1700 means that (13c) has to be measured again as the values might change.

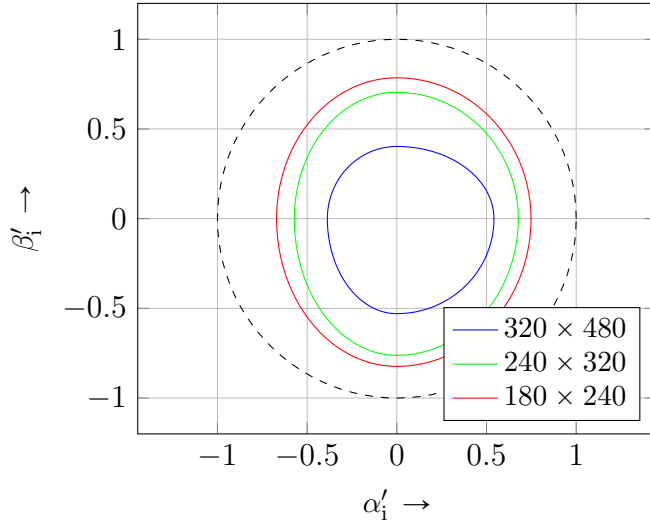


Figure 7: Maximum  $(\alpha'_i, \beta'_i)$  directions to see a certain common area of the micro mirror array (legend denotes number of common pixels seen)

## 4 Optimal Positioning

### 4.1 Optimization Strategy and Its Solution

By utilizing the mathematical description in Sec. 3 this section defines an objective to be maximized at the optimal incident angles. It is nothing more than a modified version of (12). Before going into detail some facts are pointed out. First, the experimental setup is symmetric to the  $\alpha\gamma$ -plane as well as to the  $\beta\gamma$ -plane. Symmetric in this case means that we are not interested in the output light having a positive or negative  $\beta$ -component in the DCS. As the devices normal lies within the  $\alpha\gamma$ -plane it does not matter if the input light comes from  $-\beta$ -direction, i.e.,  $\pi/2 < \varphi_i < \pi$ , and output light goes to  $+\beta$ -direction or vice versa. Another fact comes from the physical setup that there is one input laser beam from the left hand side of the DMD and one from the right hand side. The symmetry is guaranteed by the tilt of the micro mirrors to either  $\varrho = +\pi/15$  or  $\varrho = -\pi/15$ .

To set up a real optical MIMO system one shall use lasers having the same wavelength  $\lambda_{i1} = \lambda_{i2}$ . Hence both laser beams produces the same output intensity distribution on the  $\beta$ -axis and one have to calculate only one function and search for the maximum. Consequentially we define the optimization program as

$$(\theta_{i1}, \varphi_{i1}) = \arg \max_{\substack{0 < \theta_{i1} < \pi/2 \\ \pi/2 < \varphi_{i1} < \pi}} \max_{\substack{\alpha=0 \\ \beta \\ \varrho = +\pi/15}} I(\alpha', \beta', \alpha'_{i1}, \beta'_{i1}) \quad (16)$$

This optimization is highly non-convex as to be seen in Fig. 6. Therefore easy convex optimization techniques cannot be used to solve this problem. Instead we use a 'exhaustive' search to get the angle-pair  $(\theta_{i1}, \varphi_{i1})$ . The pair  $(\theta_{i2}, \varphi_{i2})$  follows directly by (4).

We choose the search domain as  $61/180 \cdot \pi \leq \theta_{i1} \leq 71/180 \cdot \pi$  and  $1/180 \cdot \pi \leq \varphi_{i1} \leq 89/180 \cdot \pi$  each direction with steps of  $0.025/180 \cdot \pi$ . For some selected wavelength we use in our testbed we figured out the optimal setup:

Table 1: Optimal incident angles on a DLP1700 chip for two lasers having the same wavelength

| $\lambda$                    | $\varphi_{i1/i2}$      | $\theta_{i1}$          | $\theta_{i2}$           |
|------------------------------|------------------------|------------------------|-------------------------|
| $633 \cdot 10^{-9}\text{m}$  | $36.000/180 \cdot \pi$ | $66.375/180 \cdot \pi$ | $113.625/180 \cdot \pi$ |
| $778 \cdot 10^{-9}\text{m}$  | $44.600/180 \cdot \pi$ | $65.650/180 \cdot \pi$ | $114.350/180 \cdot \pi$ |
| $1326 \cdot 10^{-9}\text{m}$ | $38.000/180 \cdot \pi$ | $66.375/180 \cdot \pi$ | $113.625/180 \cdot \pi$ |
| $1576 \cdot 10^{-9}\text{m}$ | $46.125/180 \cdot \pi$ | $66.000/180 \cdot \pi$ | $114.000/180 \cdot \pi$ |

From Tab. 1 one may ask if there exists an analytical description which is followed by  $(\theta_i, \varphi_i)$ , i.e., determines the incident angles as a function of the used wavelength  $\lambda$ . In a simulation figuring that out we fixed  $\theta_{i1}$  to  $11/30 \cdot \pi$  as this angle is fixed except for a small fraction of it. Now we look for solutions of (16) over different wavelengths. Finally we applied a regression on previously sorted sets of the outcome data points to obtain analytic functions of quadratic form  $\lambda = f_j(\theta_{i1} = 11/30 \cdot \pi, \varphi_i) = [\lambda_m (\varphi_{i1} - \pi/2)^2 + \lambda_o] \cdot 10^{-9}$ .

Table 2: Analytic functions of quadratic form  $\lambda = f_j(\varphi_i) = [\lambda_m (\varphi_{i1} - \pi/2)^2 + \lambda_o] \cdot 10^{-9}$  for  $\theta_{i1} = 11/30 \cdot \pi$

| $j$ | $\lambda_m[\text{nm}]$ | $\lambda_o[\text{nm}]$ | $p(\text{found points} \in f_j)$ |
|-----|------------------------|------------------------|----------------------------------|
| 1   | -311.0                 | 624.5                  | 0.0032                           |
| 2   | -354.9                 | 728.1                  | 0.0400                           |
| 3   | -415.1                 | 872.3                  | 0.0241                           |
| 4   | -507.5                 | 1088.0                 | 0.1440                           |
| 5   | -666.7                 | 1448.0                 | 0.0698                           |
| 6   | -994.0                 | 2167.0                 | 0.6815                           |
| 7   | -1604.0                | 3886.0                 | 0.0374                           |

The analytic functions as well as the data points where these functions are derived from are given in Fig. 8. The 'x'-marks give the data points we got out of our simulation. The dashed and solid curves represent the analytic function given in Tab. 2, where the solid lines are functions we also got in a prior simulation made with a more coarse goal function compared to the one defined in (16). Similar simulations with  $\theta_{i1}$  around  $11/30 \cdot \pi$  gives similar results. In the family of curves the offset  $\lambda_o$  slightly increases with decreasing  $\theta_{i1}$  and vice versa.

## 4.2 Usable Input Angles

Based on the previous considerations, a consequential question is, which angles  $\varphi_i$  are allowed to be used in the experimental setup. The idea to proceed is as follows. First we look at the incident angles we are interested in and transform them into our DCS using (3) and (11). After that is done the direction is rotated into the DMDs DCS similar to (1a). Finally we look if the angle of interest is located within the domain as shown in Fig. 7 depending on degree of restriction. This means that both input laser beams have to interface at minimum a certain common area in percentage of the whole micro mirror array. Fig. 9 shows how the angles  $\varphi_{i1/i2}$  change. The family of curves assumes  $\theta_{i1} = 11/30 \cdot \pi$  and  $\theta_{i2} = 19/30 \cdot \pi$ . The solid lines gives the area with the DMD rotated

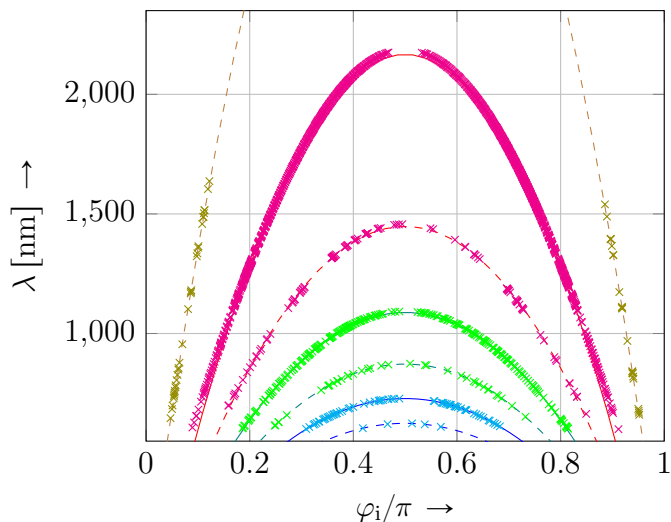


Figure 8: Analytic functions to determine optimal incident  $\varphi_i$  for a certain wavelength  $\lambda$  and  $\theta_{i1} = 11/30 \cdot \pi$

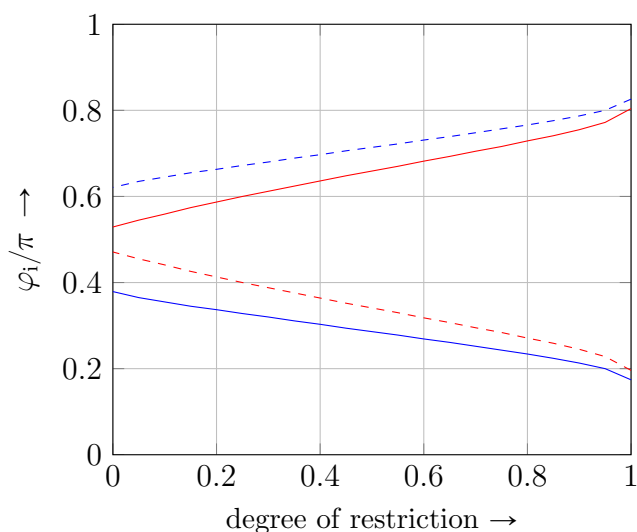


Figure 9: Usable incident angles  $\varphi_i$  for a certain minimum shared area seen by both laser beams for  $\theta_{i1} = 11/30 \cdot \pi$

with  $3/4 \cdot \pi$  and the dashed ones with  $-1/4 \cdot \pi$ . The usable area for  $\varphi_i$  is located between the solid or between the dashed curves, respectively.

In Fig. 9 one can additionally see that the area between the curves is not symmetric to  $\pi/2$  as one may expect. This is due to the fact that the micro mirror is not centered within the DLPs housing.<sup>6</sup> Hence, one has to prefer the domain  $0 \leq \varphi_i \leq \pi/2$  if the DLP is rotated by  $3/4 \cdot \pi$  to have a wider range of  $\varphi_i$  for steering the optimal incident angle to select one of the curves shown in Fig. 8.

Closing this section a trade-off is pointed out which has to be taken into account. If one look to Fig. 8, one may want to be not too sensitive to small changes in  $\lambda$ . Hence, one should choose  $|\pi/2 - \varphi_i|$  as large as possible. One the other hand, if one does so, one may not be able to use the whole micro mirror array of the DMD and has to allow a large degree of restriction.

<sup>6</sup>see also Sec. 3.3

## 5 Conclusion and Future Work

The DLP technology has been arrived in today's modern video projectors. Compared to SLM techniques for coupling light sources into a MMF in serial we use the DLP1700 to set up the input part of a  $M \times 2$  optical MIMO system in parallel. The main advantage of that SLM is that we are able to initiate two different mode groups into a MMF in parallel. The setup is as follows: two independent sources transmit data streams through a single mode fiber at whose ends collimators widen the laser light and forward them to our used DLP1700. This paper deals with the problem where to place these two collimators such that the reflected light has a common output direction. We wish to excite on a MMF low order modes with light coming from one light source and higher order modes coming from the other one simply by changing the tilt of corresponding pixels of the DLP.

Solving this issue we consider the DMD in general as a blazed grating in a first step. The prediction of the reflected light intensity distribution in front of the DMD allows us to figure out, where to place the collimators. We show that there does not exist a unique solution as well as the solution depends on the operating wavelength  $\lambda$ . In a second step we consider the housing DLP1700 specifically. The housing of the DLP1700 limits the positions where the collimators took place if one demands to use a certain common sub-array of micro mirrors. Finally, the positioning becomes a trade-off between the sensitivity in respect to the operating wavelength  $\lambda$  and the usable micro mirror array of the DLP1700.

In future work we will setup up our testbed as theoretically described here. The intensity distribution has already been retraced partway in [8] for visible light. We will redo that again and extend that for other operating wavelengths. Further, we will continue by showing that bit maps assigned to the DLP1700 can be measured at the MMF's surface if one light source impinges the DMD.

## References

- [1] A. Shah, R. Hsu, A. Tarighat, A. Sayed, and B. Jalali, "Coherent optical MIMO (COMIMO)," *Lightwave Technology, Journal of*, vol. 23, no. 8, pp. 2410–2419, Aug. 2005.
- [2] M. Greenberg, M. Nazarathy, and M. Orenstein, "Data Parallelization by Optical MIMO Transmission Over Multimode Fiber With Intermodal Coupling," *Lightwave Technology, Journal of*, vol. 25, no. 6, pp. 1503–1514, June 2007.
- [3] R. Panicker, J. P. Wilde, J. Kahn, D. Welch, and I. Lyubomirsky, "10 × 10 Gb/s DWDM Transmission Through 2.2-km Multimode Fiber Using Adaptive Optics," *Photonics Technology Letters, IEEE*, vol. 19, no. 15, pp. 1154–1156, Aug. 2007.
- [4] G. Gilder, "Plenary paper: The rise of Exaflood optics," in *Optical Communication, 2009. ECOC '09. 35th European Conference on*, Sept. 2009, pp. 1–1.

- [5] A. Chralyvy, “Plenary paper: The coming capacity crunch,” in *Optical Communication, 2009. ECOC '09. 35th European Conference on*, Sept. 2009, pp. 1–1.
- [6] R. W. Tkach, “Scaling optical communications for the next decade and beyond,” *Bell Labs Technical Journal*, vol. 14, no. 4, pp. 3–9, Winter 2010.
- [7] J. Pankow, “Entwicklung einer modenselektmode Lichtwellenleiter-Einkopplung für die optische MIMO-Übertragung auf der Basis von MEM-Chips,” Master’s thesis, University of Applied Sciences Technology, Business and Design, Dez. 2011.
- [8] S. Schröder, “Development of a mode selective coupling device for optical MIMO communications bases on the Digital Light Processort DLP 1700,” Master’s thesis, University of Applied Sciences Technology, Business and Design, Oct. 2012.
- [9] P. J. Winzer and G. J. Foschini, “MIMO capacities and outage probabilities in spatially multiplexed optical transport systems,” *Opt. Express*, vol. 19, no. 17, pp. 16 680–16 696, Aug. 2011. [Online]. Available: <http://www.opticsexpress.org/abstract.cfm?URI=oe-19-17-16680>
- [10] A. Ahrens, J. Pankow, S. Aust, and S. Lochmann, “Optical MIMO Multimode Fiber Links Channel Measurements and System Performance Analysis,” in *Optical Communication Systems (OPTICS), 2011 Proceedings of the International Conference on*, July 2011, pp. 1–5.
- [11] *DLP<sup>TM</sup> Technology: Applications in Optical Networking*, vol. 4457, 2001. [Online]. Available: <http://dx.doi.org/10.1117/12.447760>
- [12] “DLP<sup>®</sup> HVGA DDR Series 210 DMD,” Texas Instruments, Dec 2010.
- [13] J. E. Harvey and C. L. Vernold, “Description of Diffraction Grating Behavior in Direction Cosine Space,” *Appl. Opt.*, vol. 37, no. 34, pp. 8158–8160, Dec 1998.
- [14] *Using Lasers with DLP<sup>®</sup> DMD technology*, Texas Instruments, Sept 2008.